Dynamics of the Dissociation of Hydrogen on Stepped Platinum Surfaces Using the ReaxFF Reactive Force Field

Jeffery Ludwig and Dionisios G. Vlachos*

Department of Chemical Engineering and Center for Catalytic Science and Technology, University of Delaware, Newark, Delaware 19716-3110

Adri C. T. van Duin and William A. Goddard, III

Materials and Process Simulation Center, California Institute of Technology, Pasadena, California 91125

Received: October 24, 2005; In Final Form: January 7, 2006

The dissociation of hydrogen on eight platinum surfaces, Pt(111), Pt(100), Pt(110), Pt(211), Pt(311), Pt(331), Pt(332), and Pt(533), has been studied using molecular dynamics and the reactive force field, ReaxFF. The force field, which includes the degrees of freedom of the atoms in the platinum substrate, was used unmodified with potential parameters determined from previous calculations performed on a training set exclusive of the surfaces considered in this work. The energetics of the eight surfaces in the absence of hydrogen at 0 K were first compared to previous density functional theory (DFT) calculations and found to underestimate excess surface energy. However, taking Pt(111) as a reference state, we found that the trend between surfaces was adequately predicted to justify a relative comparison between the various stepped surfaces. To assess the strengths and weaknesses of the force field, we performed detailed simulations on two stepped surfaces, Pt(533) and Pt(211), and compared our findings to published experimental and theoretical results. In general, the absolute magnitude of reaction rate predictions was low, a result of the force field's tendency to underpredict surface energy. However, when normalized, the simulations show the correct linear scaling with incident energy and angular dependence at collision energies where a direct dissociation mechanism is observed. Because ReaxFF includes all degrees of freedom in the substrate, we carried out simulations aimed at understanding surface-temperature effects on Pt(533). On the basis of the results on Pt(533)/Pt(211), we studied the reaction of hydrogen at normal incidence on all eight surfaces in a range of energies where we anticipated the force field to give reasonable qualitative trends. These results were subsequently fit to a simple linear model that predicts the enhanced reactivity of surfaces containing 111-type atomic steps versus 100-type atomic steps. This model provides a simple framework for predicting high-energy/high-temperature kinetics of complex surfaces not vicinal to Pt(111).

1. Introduction

Understanding the interaction of molecular hydrogen with transitional metal surfaces has been the focus of much recent experimental and theoretical work because of its importance in many chemistries, including hydrogenation reactions, on-board hydrocarbon reforming, and preferential oxidation reactions for hydrogen-purification needs in fuel cells. The interaction of hydrogen with platinum surfaces is an interesting case because the dissociation reaction

$$H_2 + 2* \rightarrow 2H* \quad (1)$$

is in general nonactivated[1,2] and exhibits an interesting non-monotonic behavior as a function of reactant energy on some crystal facets.[3,4] From a theoretical point of view, this creates several unique challenges because the typical methods for studying catalytic reactions, density functional theory (DFT) used in conjunction with a saddle-point-seeking algorithm and transition state theory (TST), cannot be used. Instead of simply being able to perform electronic structure calculations on a single configuration, one needs to map out a dynamically relevant region of the potential energy surface (PES) using DFT, parametrize this PES into either an analytic expression or an interpolating function, and finally, perform classical, quasi-classical, or quantum molecular dynamics calculations to obtain an estimate of reactivity (see review of Bonn et al.[5]).

Obtaining the PES is, in all but the most trivial cases, a difficult undertaking because of the computational demands of the DFT calculations and the high number of degrees of freedom in gas−surface systems. For the base case of Pt(111), a 6D PES, which only includes the degrees of freedom of the impinging hydrogen molecule, has yielded results that agree quite well with molecular beam experiments.[6] In previous work,[1] we used a small DFT training set with a 6D analytic potential function and obtained reasonable results, considering the limitations of the PES that we employed.[1] (See Persson et al.[7] for the technique applied to H_2/Cu(111).) A more accurate PES based on a corrugation reduction procedure[8] in conjunction with quantum molecular dynamics[6] yielded agreement with experiment, which is as good as can be expected, given the known limitations in the functionals used in modern DFT calculations.

Recently, Olsen and McCormack[9−11] have extended the corrugation reduction approach to Pt(211), a stepped surface.

* To whom correspondence should be addressed. E-mail: vlachos@che.udel.edu.

10.1021/jp0561064 CCC: $33.50
Published on Web 02/07/2006

They obtained remarkable agreement with molecular beam experiments on Pt(533)[3] using a simple geometric scaling correction to compare the two surfaces. The extension from flat, single-crystal surfaces to stepped surfaces is an exciting first step in bridging the materials gap and studying surfaces more representative of what is encountered in industrial practice. However, Pt(211) still has a relatively small unit cell, and extending the 6D PES approach to larger systems is problematic. Performing the DFT calculations becomes computationally intractable, and each new surface being considered requires a recalculation and reparametrization of a PES unique to the facet being studied. Because of the frozen substrate approximation, it is also impossible to capture surface-temperature effects that, although small, were present at low incident energies on Pt(533)[3] and may play a role in the stabilization of rougher surfaces.

In principle, a transferable atomistic force field, including all degrees of freedom, solves many of the aforementioned problems and opens up more possibilities for simulation. Surfaces of arbitrary complexity could be studied using potential parameters taken from a small training set. The major nontrivial problem is, of course, the potential's accuracy: Is the potential capable of producing reasonable dynamics on systems outside of its training set? In this work, we explore and evaluate the performance of a reactive force field, ReaxFF,[12] in simulating the reaction of hydrogen with eight platinum surfaces: Pt(111), Pt(100), Pt(110), Pt(211), Pt(311), Pt(331), Pt(332), and Pt(533). We start by comparing surface energies to published local density approximation (LDA) DFT calculations by Feibelman.[13] Next, we compare our simulation results on a single crystal, Pt(533), to the experimental work of Gee et al.[3] and the theoretical work of Olsen and McCormack[9−11] to gain insight into where the potential performs well and where it may be problematic. Finally, we simulate the dynamics on all eight crystals and develop a linear sticking model that describes the sticking behavior at normal incidence over the range of systems considered in this work.

2. Computational Methods

2.1 Overview of ReaxFF. ReaxFF is a reactive force field based on a bond order/bond distance relationship, a concept introduced by Tersoff[14] and extended to carbon chemistry by Brenner.[15] The force field operates by updating bond orders at every molecular dynamics step and therefore provides a mechanism for bonds to form and break over the course of the simulation. The original parameters and functional forms were developed to describe gas-phase reactions involving hydrocarbons[12] but were more recently extended to include metals and transition metals.[16,17] Additionally, it has been successfully applied to the study of magnesium hydrides,[18] polymer decomposition,[19] silicon/silicon oxide systems,[20] high-energy materials,[21−23] all-carbon materials,[24,25] boron nitrides,[26,27] and lithium carbides.[28] This broad range of materials demonstrates the transferability of the ReaxFF method and indicates that ReaxFF should be able to describe the complicated reaction chemistry at the interfaces between different materials. Current ReaxFF development is aiming to combine the first-row elements and the metal/metal oxide ReaxFF descriptions, which would enable us to describe catalytic reactions at metal/metal oxide surfaces. As part of this development, we have derived ReaxFF parameters for Pt and Pt/H interactions, which can be found in tables in the appendix section of this work. These parameters were optimized to reproduce the following training set obtained from quantum mechanical (QM) calculations:

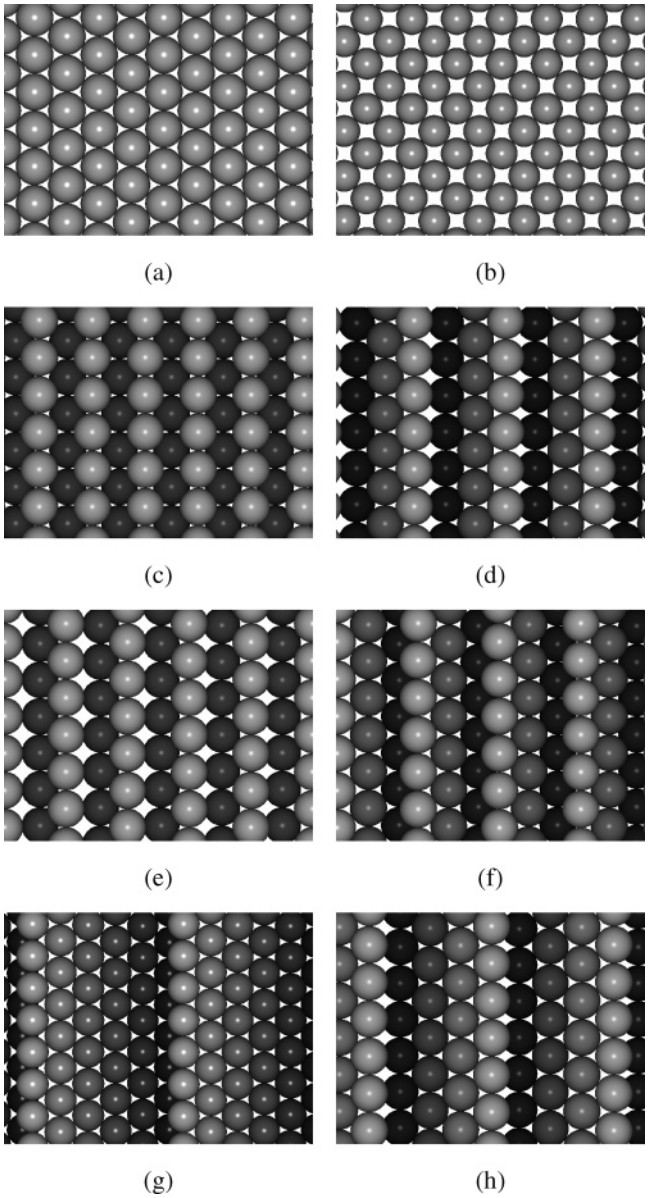

Figure 1. Surfaces considered in this study. (a) Pt(111), (b) Pt(100), (c) Pt(110), (d) Pt(211), (e) Pt(311), (f) Pt(331), (g) Pt(332), and (h) Pt(533). The lighter atoms are toward the top and the darker atoms are toward the bottom.

equations of state for fcc, bcc, a15, and simple cubic and diamond Pt-metal phases; binding energies for Pt_3 to Pt_{35} clusters; hydrogen binding energies on Pt(111) surfaces (top, bridge, fcc, hcp, and subsurface sites); H−Pt bond dissociation energies from a $(H_3N)_2PtHCl$ cluster; H_2 dissociation on a flat Pt_{12} cluster; and H_2 dissociation, $H_2 + H \rightarrow H + H_2$ reaction.[12]

We found that ReaxFF gives a good reproduction of all of these QM data. Here, we aim to establish whether the ReaxFF potential can describe H_2/Pt-surface interactions for configurations that are not included in its training set. To that end, we have studied the dynamics of H_2 dissociation at different kinetic energies with a range of Pt surfaces.

2.2 Surface Structures and Equilibration. The eight flat and stepped platinum surfaces on which ReaxFF was used are shown in Figure 1. These surfaces were chosen because they are representative of systems that have been studied both experimentally[3,29−37] and theoretically.[9,11] The surfaces are divided into three groups: flat surfaces (Pt(111) and Pt(100)), surfaces with a 100-type atomic step (Pt(211), Pt(311), Pt(533)),

TABLE 1: Notation and Geometric Parameters for Surfaces Considered in This Study

Miller index notation	# of atoms	a_1 [Å]	a_2 [Å]	area [Å][a]	stepped notation[b]
Pt(111)	48	9.73	5.62	54.71	N/A
Pt(100)	56	7.96	7.96	67.25	N/A
Pt(332)	70	13.20	5.64	74.43	Pt(S)-[6(111) × (111)]
Pt(533)	100	18.45	5.63	103.77	Pt(S)-[4(111) × (100)]
Pt(211)	72	13.80	5.63	77.71	Pt(S)-[3(111) × (100)]
Pt(331)	64	12.26	5.64	69.13	Pt(S)-[3(111) × (111)]
Pt(311)	48	9.32	5.62	52.40	Pt(S)-[(111) × (100)]
Pt(110)	60	11.92	5.64	63.36	Pt(S)-[(111) × (111)]

[a] Direct lattice vectors (a_1 and a_2) and area are relaxed values. [b] [*n*(*jkl*) × (*abc*)] indicates *n* rows of terraces of *jkl*-type with an *abc*-type atomic step.

and surfaces with a 111-type step (Pt(110), Pt(331), Pt(332), Pt(311)). Pt(311) is a bit unusual because it has both 100- and 111-type atomic steps without a terrace.

In all cases, the surfaces were considered without reconstruction, although many of these surfaces would in fact reconstruct at room temperatures in the absence of adsorbates. This was done in an attempt to develop a fundamental understanding of the relationship between the topographic features of these surfaces (111-type steps vs 100-type steps, for example). For reference, Table 1 lists these surfaces in standard Miller Index notation alongside a stepped surface notation used by Somorjai,[38] ordered from the least corrugated surface to the most corrugated surface.

The surfaces were generated using an automated script and were in all cases taken to be six-atom-thick slabs, periodic in the $x-y$ plane, and initially positioned at experimental bulk spacing. As the dynamics were carried out in a 3D periodic simulation, the spacing between slabs in the *z* direction was set to 120 Å to give a system of essentially noninteracting slabs. The unit cell was taken to be as large as possible given computational time constraints to allow for potential hot-spots to develop on crystals, which could have enhanced reactivity. Gaussian noise with a variance of 0.1 Å and a mean of zero was introduced to the initial bulk positions to avoid local minima due to symmetric initial conditions. The crystal was then heated in an NVT simulation for 50 ps using a velocity Verlet algorithm[39] with a 0.1 fs time step and a Berendsen thermosat[40] with a temperature of 500 K. This temperature was chosen to provide rapid equilibration without completely melting the crystal or causing surface reconstructions to occur. The slab was then minimized with respect to atomic positions and the $x-y$ unit cell dimensions using a conjugate gradient technique to obtain a minimum in energy at 0 K. This 0 K crystal was used in comparison to LDA−DFT calculations of surface energy as an initial benchmark of the potential. The number of atoms in each unit cell and the direct lattice vectors as well as the relaxed size of the unit cell are given in Table 1. Considering the average nearest-neighbor spacing in the $x-y$ plane, we calculated an effective lattice parameter of 3.98 Å, 1.5% larger than the experimental lattice parameter of 3.92 Å[41] but in good agreement with recent generalized gradient approximation (GGA) DFT calculations using several different functionals and computer codes.[42]

3. Surface Energetics

The potential energy of our 0-K-relaxed surfaces were compared to quantum mechanical calculations performed on system configurations not included in ReaxFF's initial training set. Table 2 compares our calculated energies for flat and stepped surfaces in the absence of hydrogen with DFT calculations at the LDA level of theory performed by Feibelman.[13] Surface energies, E^{SURF} are calculated according to

TABLE 2: Energies for Surfaces Considered in This Study[a]

surface	ReaxFF E^{SURF}	ReaxFF ΔE^{SURF}	LDA E^{SURF} [b]	LDA ΔE^{SURF} [b]
Pt(111)	2.232	0.000	2.972	0.000
Pt(110)	2.670	0.438		
Pt(311)	2.672	0.440		
Pt(331)	2.613	0.381	3.433	0.461
Pt(211)	2.587	0.355	3.410	0.438
Pt(533)	2.525	0.293	3.318	0.346
Pt(100)	2.515	0.283		
Pt(332)	2.443	0.211		

[a] Units are in kcal/mol/Å^2. [b] LDA values from ref 13.

$$E^{SURF} = \frac{E^{SLAB} - nE^{BULK}}{2A} \quad (2)$$

where E^{SLAB} is the potential energy of our system at 0 K, *n* is the number of atoms in the unit cell, *A* is the unit-cell area, and E^{BULK} is the energy of a single Pt atom in a relaxed-bulk crystal. The unit-cell area is taken to be the projection of the relaxed unit cell onto the $x-y$ plane; the effects of corrugation on surface area are neglected. The factor of 2 in eq 2 accounts for the fact that the slab has two exposed surfaces contributing to surface energy. When using electronic structure methods to calculate surface energy, this definition of surface energy may be linearly divergent.[43] Because we are using an atomistic potential instead, where differing *k*-point meshes and basis sets between bulk and slab calculations are not an issue, we believe this definition of surface energy is adequate.

Comparing the absolute magnitude of these numbers, we find a systematic error of approximately −0.75 kcal/mol/Å^2 versus the reported LDA values. This may be attributable to a discrepancy in the level of theory used in each case; the ReaxFF force field was trained on DFT cluster calculations at the GGA level of theory using the B3LYP functional versus the LDA level of theory employed by Feibelman. The energies are normalized to surface area and are therefore a good measure of their relative stabilities. Unstable surfaces have high energies and stable surfaces have low energies. Intuitively, one would expect a less stable surface to be more reactive. Therefore, if the LDA values are more accurate than the force field predictions, we would expect to systematically underestimate reactivity.

Instead of comparing absolute numbers, if we look at surface energy using Pt(111) as a reference state ($E^{SURF} = 0$), then the agreement with the trend in Feibelman's LDA calculations is quite good. These results, shown in Figure 2 and Table 2 as ΔE^{SURF}, indicate that even if the absolute values of surface energies have a systematic error, we should be able to gain some insight into the reactivity differences between the various topographic features because the relative energies are in good agreement. For this reason, we believe the simulations presented here are best interpreted by examining the qualitative and quantitative differences between the facets using flat surfaces as base cases for comparison.

4. Molecular Dynamics

4.1 Initial Conditions and Classification of Trajectories. The coordinate system used in the molecular dynamics simulations is given in Figure 3. Prior to performing trajectories, the minimized 0 K slabs used in comparison with quantum results

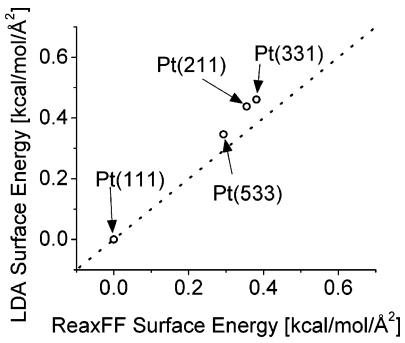

Figure 2. LDA surface energies vs ReaxFF surfaces energies. Pt(111) is taken as a reference point ($E^{Pt(111)} = 0$). The dotted line is $y = x$.

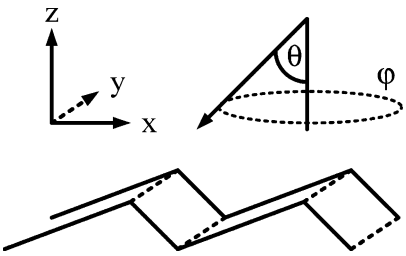

Figure 3. Coordinate system used in classical trajectory studies. Stepped surfaces are aligned so that the step and terrace normals are in the $x-z$ plane. The incident angle $\theta = 0$ corresponds to trajectories that impinge the normal to the $x-y$ plane; $\theta > 0$ impinge on the step edge, and $\theta < 0$ impinge on the terrace. The azimuthal angle φ is kept at zero in this work, which corresponds to the zero y component of the momentum.

were reequilibrated back to the target surface temperature, which is 300 K (unless specified otherwise), in an NVT ensemble. These equilibrated positions and velocities were used as the initial conditions of the substrate atoms in the trajectory studies. At the start of a trajectory, the center of mass of a hydrogen molecule was located randomly in the unit cell, 5 Å above the highest atom on the substrate. The molecule was oriented randomly by rotation about its x and z axes.

The initial kinetic energy of the hydrogen molecule was partitioned into two parts: center of mass energy E_{COM} and internal energy. We define center of mass energy as follows:

$$v_{COM} = \left|\left|\frac{1}{M}(m_1\mathbf{v}_1 + m_2\mathbf{v}_2)\right|\right| \quad (3)$$

$$E_{COM} = \frac{1}{2}Mv_{COM}^2 \quad (4)$$

where v_{COM} is the velocity of the center of mass, M is the total mass of the hydrogen molecule, and m_1, m_2, v_1, and v_2 are the masses and velocities of the individual hydrogen atoms, respectively. In this work, we only consider trajectories with momentum orthogonal to the atomic step edge so that the y component of momentum is always zero. The momenta in the x and z directions are then chosen to yield the proper incident angle θ (Figure 3).

The only internal energy considered in this study was the $v = 0$ vibrational mode, the zero-point energy (ZPE) of a hydrogen molecule in the gas phase. Excluding the internal rotational motion in our simulations is justified because expansion in the nozzles of the molecular beam equipment tends to transfer energy from the rotational modes into translation.[44] If we include the zero-point energy in our initial conditions, then the simulation will be called quasi-classical, whereas if this energy is omitted (no internal motion), then the simulation will be called classical. The value of the ZPE ($^1/_2\hbar\omega_0$), 0.274 eV, was taken from the calculations of Kolos and Wolniewicz.[45] Both types of simulations were conducted to understand the effects of initial conditions on dynamics. The reasons for including or omitting this energy when performing molecular dynamics simulations are discussed in more detail by McCormack et al.[11] In summary, the key problem with always including the ZPE is that the energy cannot be contained in its vibrational mode but instead is free to transfer to other internal or translational motions. This may be physically impossible in the real system because of quantum mechanical constraints. This extra energy is available to the molecule to escape weakly bound precursor states that may be critical to accurately describing the dynamics. For this reason, if we were performing trajectories in a region where we expect precursor states or long-lived intermediates to be significant (less than 2.0 kcal/mol incident energy, on the basis of experiments on Pt(533)),[3] then we omitted the ZPE. However, at higher-incident energies when the dissociation occurs via a direct mechanism, we included the ZPE because it tends to reduce simulation time.

After all initial conditions were specified, NVE trajectories were integrated using a velocity Verlet algorithm with a 0.1 fs time step. This time step conserved the total energy to within 0.1 kcal/mol, and we found that decreasing the time step did not affect the reaction probability within statistical error. Trajectories were continuously monitored during the simulation until each trajectory was classified in one of three ways. If the hydrogen molecule's bond length exceeded 3.0 Å, then the trajectory was considered dissociated. In the gas phase, previous quantum mechanical studies[1,7] have shown that the bond energy at a separation distance of 3.0 Å is effectively zero. If the center of mass of the hydrogen−hydrogen bond exceeded its initial height above the surface by 5 Å, then the trajectory was considered reflected. Again, previous quantum mechanical studies have shown that the Pt slab and hydrogen molecule do not interact at this distance.[1,7] In contrast to recent classical trajectory studies by McCormack et al.[11] and other 6D-PES-based approaches, we had a third dynamic possibility. By exchanging kinetic energy with the surface, the molecule could become trapped in a molecularly physisorbed state. This is a unique feature of these simulations and is not a possible feature within the frozen-substrate approximation typically employed. To determine if a trajectory had become trapped, we picked an arbitrary cutoff time of 100 ps as a maximum simulation time, without observing either a dissociation event or a reflection event. At low incident energies, low surface temperatures, and excluding ZPE from our initial conditions, these trapped trajectories did become important, at times accounting for 30% of the reactive trajectories. At higher temperatures, collision energies, and with the inclusion of ZPE, these trapped trajectories were seldom observed. Because any trajectories not reflecting off of the surface in a molecular beam experiment would be seen as reactive, we use the term sticking coefficient to include both directly dissociated and molecularly trapped trajectories. Movies of sample reflected, dissociated, and trapped trajectories are available (Supporting Information). The convergence of the sticking coefficient as a function of the number of trajectories is shown in Figure 1S (Supporting Information).

After the trajectory was classified, the process was iterated until the error estimate on the percentage of sticking trajectories was acceptably low. This required averaging over a large number of trajectories, usually between 2000 and 5000 for a given incident energy because reaction probabilities were

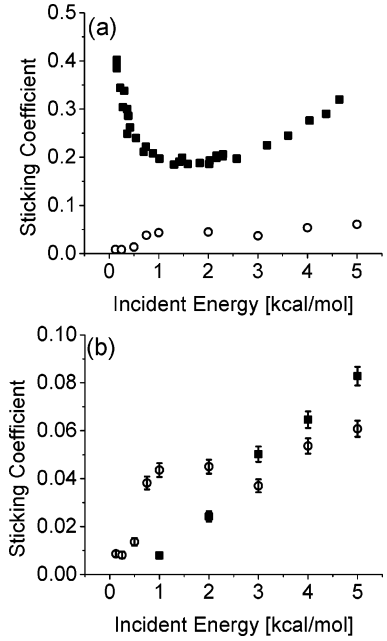

Figure 4. (a) Sticking coefficient of H_2 as a function of the incident energy at normal incidence on Pt(533). The filled squares are the experimental data of Gee et al.[3] and the open circles indicate the simulation results using classical sampling. (b) Comparison of classical sampling (open circles) vs quasi-classical sampling (closed-squares) over the same energy range.

typically below 10%. We used the Wald confidence interval[46] with $\alpha = 0.6827$ for all error estimates.

4.2 Pt(533) and Pt(211). *4.2.1 Normal Incidence.* Gee et al.[3] have performed molecular beam experiments on the H_2/Pt(533) system. Experimental data obtained by varying the incident energy of molecules while keeping the beam aligned normal to the surface are shown in Figure 4a. Initially, the sticking probability is fairly high, then it begins to decrease as energy is increased, and then increases again in a linear fashion when the incident energy exceeds 2 kcal/mol. The source of this nonmonotonic behavior has been discussed at length elsewhere.[3,9−11] In summary, the experiments show that at very low energies, a temperature-dependent precursor mediated mechanism dominates. As energy increases a little more, a temperature-independent precursor mechanism becomes relevant. Dissociation via both of these precursor-mediated indirect pathways decreases with increasing collision energy because eventually, most molecules are too energetic to become temporarily trapped in a weakly bound molecular state. A third mechanism, a direct dissociation mechanism, which scales linearly with energy, begins to dominate the dynamics at approximately 2.0 kcal/mol incident energy and is very similar to the behavior seen on flat Pt(111) crystals.[47,48] The initial decline with increasing collision energy is therefore the result of the indirect pathway being shut off, and the eventual increase is due to the direct channel becoming more important.

Comparing our classical simulations (which do not include ZPE in the initial conditions) with experiment (Figure 4a), we find our predicted sticking probabilities are much too low over the entire range of energies studied experimentally. At an energy of 2.0 kcal/mol, a region representative of the transition from the indirect pathway to the direct pathway, we underestimated the sticking probability by a factor of 4. This result was somewhat anticipated, given our force field's under-prediction of surface energy (section 3) and a slight activation barrier (approximately 2 kcal/mol) in the QM training set for ReaxFF.

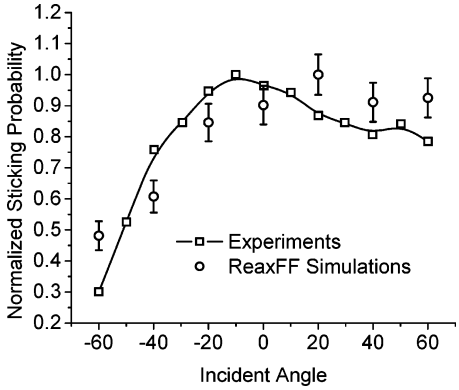

Figure 5. Sticking probability from the simulation vs the molecular beam experimental data from Gee et al.[3] (max values normalized to 1.0). The solid line connects experimental points for clarity. Error bars on simulations (circles) represent one standard deviation.

In our simulations, we did begin to see some signs of nonmonotonic behavior at lower energies when using classical initial conditions (see Figure 4b for details of the simulation data shown in Figure 4a), but we did not observe a steady increase in reaction probability when incident energy was decreased. Rather, we saw a maximum near 2.0 kcal/mol that then began to decrease as incident energy decreased. The simulations of McCormack et al.[11] did not exhibit this drop off of reaction probability at low incident energies. We attribute some of this discrepancy to finite temperature effects (section 4.2.3), but it is most likely due to deficiencies of the potential in describing some of the low-energy pathways to dissociation.

Figure 4b compares the classical and quasi-classical initial conditions for the Pt(533) system. Including the ZPE eliminates the presence of nonmonotonic behavior and results in predictions that show a trivial reactivity below 1.0 kcal/mol incident energy. As expected, the inclusion of ZPE eliminates the ability of the molecule to enter weakly bound precursor states and confines the dynamics to the direct pathway. Including ZPE does however obtain the correct linear scaling of sticking probability with incident energy. For this reason, we will focus most of our remaining efforts on the higher-energy pathways, where the quasi-classical trajectories and ReaxFF seem to give a realistic qualitative description of the dynamics.

4.2.2. Effect of Incident Angle. We have performed simulations varying the incidence angle and keeping the collision energy fixed in the direct-dissociation region ($E = 5.0$ kcal/mol). As before, our absolute magnitudes of the sticking coefficient are low, and therefore, we only compare the normalized results using quasi-classical sampling to the experiments (Figure 5). The potential performs well in obtaining the proper qualitative trend. At negative values of incidence (Figure 3), the hydrogen molecules impinge mostly on the terrace of the Pt(533) surface. As the angle is increased, the reaction probability increases until it reaches a maximum when the trajectory is incident on the atomic step. We find it interesting that although the step seems slightly more reactive, the dissociation probability is relatively constant over incident angles ranging from -20 to 60° in both experiments and simulations (including those of Olsen and McCormack[9−11]). Only when the step is completely shadowed do we see a noticeable drop in reaction probability.

4.2.3. Temperature Effects. Because we included substrate degrees of freedom in our simulations, we attempted to simulate the temperature-dependent precursor state found at very low energies. Gee et al.[3] report that increasing surface temperature decreased sticking probability at very low collision energies

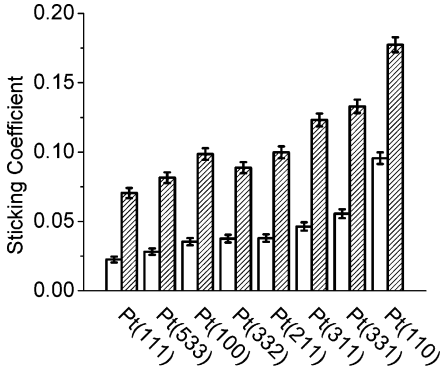

Figure 6. Sticking coefficient of all crystals as a function of energy at normal incidence using quasi-classical sampling. The unfilled columns are the simulations performed at 2.0 kcal/mol incident energy and the hatched columns are the simulations performed at 5.0 kcal/mol. The error bars are one standard deviation on the basis of a Gaussian approximation to the binomial distribution.

TABLE 3: H_2/Pt(533) Effect of Surface Temperature on the Sticking Coefficient as a Function of Incident Energy

T^{SURF} [K]	$E = 0.152$ [kcal/mol]	$E = 4.15$ [kcal/mol]
150	0.0085	0.0535
400	0.0070	0.0595

(0.15 kcal/mol) and slightly increased sticking probabilities at intermediate (0.41 kcal/mol) and high (4.15 kcal/mol) collision energies. We performed classical simulations at two temperatures, 150 K and 400 K, for both the lowest and highest energies considered by Gee et al. The results of the average of 2000 trajectories are shown in Table 3. We do, in agreement with experimental trends, see negative temperature dependence at low energies, where a precursor-mediated mechanism dominates, and a very slight positive temperature dependence at much higher energies associated with the direct pathway. When increasing the temperature, the percentage of sticking trajectories that are molecularly trapped (as opposed to directly dissociated) drops from 29% at 150 K to 7% at 400 K, indicating that we are in fact observing a temperature-dependent physisorbed molecular precursor.

This accounts for some of the discrepancy between our simulations and those of McCormack and Olsen[9−11] because using a surface temperature of 0 K would have increased our sticking probability at lower energies. However, this temperature effect is not sufficiently large to completely account for the qualitative differences between our work, experiment, and previous 6D simulations in the precursor regime. Rather, the problem is most likely due to an inadequate description of the indirect pathway by the force field. This is not surprising because ReaxFF was trained on favorable low-energy direct dissociation channels that do not resemble the tortuous and convoluted pathways followed in the indirect channel. For a more thorough description of the indirect channel, see the recent dynamic study by McCormack et al.[11] With additional training points, it may be possible to retrain the force field to more accurately capture the behavior in the precursor regime.

4.3. All Crystals. *4.3.1. Collisions at Normal Incidence and the Reactive Site.* We performed simulations on eight stepped surfaces considering only normal collisions at two different energies in the direct-dissociation regime, $E = 2.0$ and 5.0 kcal/mol, using quasi-classical sampling (ZPE was included). The results shown in Figure 6 show a clear trend with a few exceptions. The least reactive surfaces are flat or stepped surfaces with almost fully coordinated step-edge atoms. Pt(111) is the least reactive, followed by Pt(533), which has the second lowest step density of the surfaces considered. The most reactive surfaces are the highly corrugated surfaces with undercoordinated step-edge atoms, with unreconstructed Pt(110) topping the list. There also exists a second, more subtle trend. Surfaces with a 111-type step tend to more be reactive than their 100-type stepped analogues. For example, Pt(332) is more reactive than Pt(533), although it has a lower step density, and Pt(331) is more reactive than Pt(211), which has exactly the same terrace configuration. Increasing incident energy from 2 to 5 kcal/mol (a factor of 2.5), we find that the sticking coefficient increased by a factor of 2.6, almost uniformly over all surfaces. We are observing near linear scaling with incident energy. This will be discussed in more detail later in the context of a linear sticking model.

It is also interesting to examine where the reaction is taking place. Figure 7 shows a histogram of reaction probability along a direction normal to the step edge (the x axis). The site of reaction is taken to be the center of mass of the H−H bond when the bond length reaches 3.0 Å. The reported frequencies are averaged over the direction parallel to the step, which is a mixture of the top, hollow, and bridge sites. The two flat surfaces, Pt(111) and Pt(100), show an essentially uniform distribution of reaction probability, the differences essentially being Gaussian noise. This distribution is what one would expect for surfaces exhibiting no preferential site for dissociation. Even Pt(110), with its steps packed very close together, showed no preference for a dissociation site. As the spacing between steps increased, a preference for the site situated on top of the step atom is observed. This site has previously been identified as the reactive site for Pt(332),[31] Pt(553),[31] Pt(533),[3] and Pt(211).[9−11] In all surfaces with at least a three-atom terrace region, we see

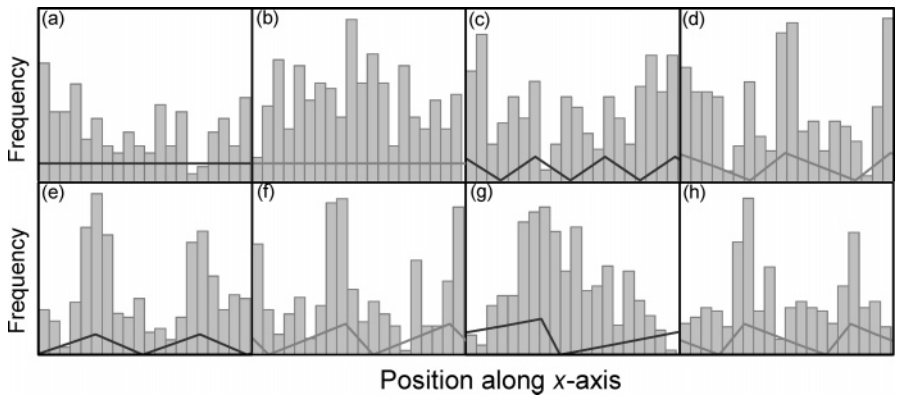

Figure 7. Histogram of dissociation probability as a function of location along a direction normal to step edge. The solid lines are the side profile of crystal surfaces ($x-z$ plane). (a) Pt(111), (b) Pt(100), (c) Pt(110), (d) Pt(211), (e) Pt(311), (f) Pt(331), (g) Pt(332), and (h) Pt(533).

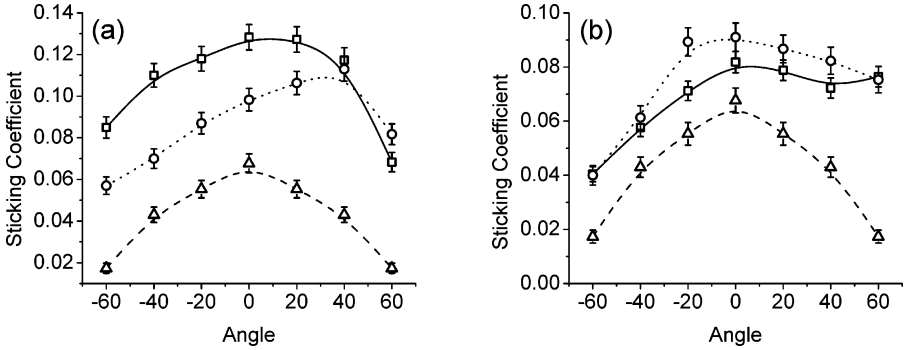

Figure 8. Sticking coefficient as a function of incident angle (see Figure 3 for the coordinate system) using quasi-classical sampling and an incident energy of 5.0 kcal/mol. (a) Pt(331) (squares), Pt(211) (circles), and Pt(111). (triangles). (b) Pt(533) (squares), Pt(332) (circles), and Pt(111) (triangles). The lines are spline fit to simulation data to guide the eye.

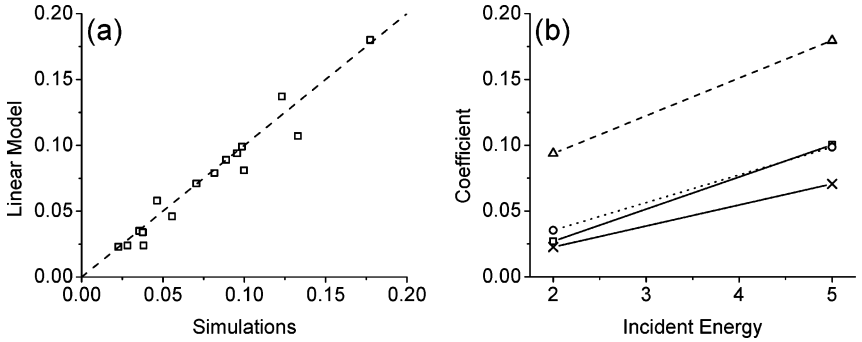

Figure 9. Linear sticking model results. (a) The open squares are simulation results vs the linear model fit for $E = 2.0$ and $E = 5.0$ quasi-classical initial conditions. The dotted line is the $y = x$ line. (b) Linear model coefficients as a function of incident energy: open squares: s^{S}_{100}, open circles: s^{T}_{100}, open triangles: s^{S}_{111}, and crosses: s^{T}_{111}.

a clear preference for this top-of-step site, with Pt(533) proving to be the most spatially selective of all of the surfaces considered.

4.3.2. Angular Dependence. We have compared the angular dependence of the sticking coefficients of Pt(331) (Pt(S)-[3(111) × (111)]) against Pt(211) (Pt(S)-[3(111) × (100)]), and Pt(332) (Pt(S)-[6(111) × (111)]) against Pt(533) (Pt(S)-[4(111) × (100)]). The simulation results, shown in Figure 8 against Pt-(111) as a reference, all follow the same basic functional form, which was observed experimentally on Pt(533)[3] (also see Figure 5). The presence of a step on a surface seems to cause the 111-type terrace regions to be more reactive toward dissociation than unmodified Pt(111). That is, there is some evidence for coupling between the steps and terraces, albeit weak. But as the increase in reactivity at positive incident angles shows, the steps themselves contribute substantially to the overall reaction. We see again that the 111-type steps are more reactive than their 100-type counterparts: Pt(331)'s terrace region is more reactive than that of Pt(211). It is not possible to generalize in the Pt-(332) versus Pt(533) case, but despite having a lower step density, Pt(332) is more reactive over the entire angular range.

4.3.3. Linear Sticking Model. To examine the trends between the crystal surfaces, the simulation results for the reaction at normal incidence using quasi-classical initial conditions and incident energies of 2.0 and 5.0 kcal/mol were fitted to a simple linear model based on the fraction of a surface consisting of a given topology.

$$s = s^{S}_{100} f^{S}_{100} + s^{T}_{100} f^{T}_{100} + s^{S}_{111} f^{S}_{111} + s^{T}_{111} f^{T}_{111} \qquad (5)$$

where s is the sticking coefficient, f is the fraction of the surface occupied by the specified crystal feature, superscripts S and T stand for step and terrace, and the subscripts refer to 111-type or 100-type steps or terraces. For example, f^{T}_{100} is the fraction of the surface covered by 100-type terraces, and s^{T}_{100} would be the nominal sticking coefficient on that crystal feature. The fractions are taken to be the surface area on the basis of a projection onto the $x-y$ plane (we do not account for corrugation) because we modeled only normal collisions. (This is the same convention used to calculate surface energies.) Including off-normal collisions, one would need to take into account the effects of shadowing through some sort of angular dependence in the model coefficients. The four s parameters on the RHS of eq 5 are all a function of incident energy. In the model fit, we only treat the two step coefficients as adjustable parameters: s^{S}_{100} and s^{S}_{111}. The coefficients for the corresponding terrace regions are taken to be the nominal values on Pt(100) and Pt-(111), respectively, without adjustments.

TABLE 4: Coefficients Used in the Linear Sticking Model of Quasi-Classical Simulation Data

	energy [kcal/mol]		
	2.0	5.0	slope [mol/kcal][a]
s^{S}_{100}	0.0271	0.1003	0.0244
s^{T}_{100}	0.0354	0.0986	0.0211
s^{S}_{111}	0.0938	0.1796	0.0286
s^{T}_{111}	0.0226	0.0706	0.0160

[a] Slope is $\Delta c/\Delta E \approx dc/dE$, where c is the coefficient of interest and E is the incident energy.

The results of our model fit and its comparison to simulation results are shown in Figure 9a, and the fit coefficients can be found in Table 4. This very crude model performed well in capturing the trends in the simulation results, in light of the fact that the model has only two degrees of freedom. Once again, considering Pt(533) in detail, at an incident energy of 2.0 kcal/

mol, we find that 28% of the surface area is covered by a 100-type step, which accounts for 32% of total sticking. This is higher than the 17% estimated by Gee et al.[3] by deconvoluting angular sticking data but close to the simulation results of Olsen and McCormack.[9−11] Comparing the relative magnitudes of the coefficients in Table 4, the 111-type steps show enhanced reactivity toward direct dissociation at both collision energies, which is consistent with previously mentioned trends. Surveying the literature for experimental evidence of this phenomenon, we find that Salmeron et al.[31,37] have performed hydrogen−deuterium exchange reaction experiments on Pt(332) and Pt(553) (one terrace row smaller than the Pt(332) surface considered in this study). When comparing these two surfaces with 111-type steps, to the results on Pt(533)[3], which has a 100-type step, the 111-type steps do in fact show enhanced reactivity. In their analysis, Gee et al.[3] estimate that Pt(553) is roughly 1.7 times more reactive than the Pt(533) surface. At an incident energy of 2.0 kcal/mol, our linear model predicts Pt(553) to be approximately 1.5 times more reactive than Pt(533), in good agreement with experimental observations.

When considering the behavior over all of these surfaces, it becomes clear from both experiments and simulation that in an energetic region where direct dissociation is likely to occur, the steps are not causing an order of magnitude increase in reactivity. The reactivity of the steps to direct dissociation appears to be only slightly higher (100-type step) or at most, increased by a factor of 3 (111-type step).

Figure 9b shows the change in the model coefficients as a function of energy. We find that the coefficients, like the overall sticking probability, tend to scale linearly, almost with the same slope (Table 4). Implicit in using a linear functional form is an assumption that the reactivity is proportional to the initial site of impact. It assumes a direct mechanism for dissociation. It is for this reason that we believe this model works in the energy ranges considered here. We can think of the reactivity of a complex corrugated surface as a simple linear combination of topographic features, provided the molecules have enough incident energy to dissociate through a direct mechanism. The validity of such a simple model enables one to predict the average sticking probability of surfaces with very low misorientation, that is, low step density with respect to (100) or (111) crystallographic planes, which are computationally intractable even for molecular dynamics. If the molecule dissociates via an indirect mechanism, where molecules lose memory of their initial configuration prior to dissociation, the sticking probability will not be proportional to the surface area but involve coupling between step and terrace regions.

5. Conclusions

We have studied the reaction of hydrogen with flat and stepped platinum surfaces using a transferable reactive force field. Given that no retraining of the potential was done to account for the specific systems studied here, we believe that ReaxFF has performed well in helping us to understand the qualitative differences between the eight surfaces considered in this work. Including the substrate degrees of freedom allowed us to account for substrate-temperature effects and survey a large number of surfaces vicinal to Pt(111) without performing any additional quantum mechanical calculations. When considering only the quantitative performance, ReaxFF offered predictions for surface energy and reactivity that were too low. Additionally, the trend in the low energy regime of the dissociation reaction on Pt(533) was not captured properly. However, the potential did a good job of capturing the high-energy direct dissociation mechanism, and it remains possible that a retraining of the potential with configurations more representative of the indirect channels might yield accurate qualitative behavior in the low-energy regime while preserving the correct dynamics in higher energy areas. If accurate, absolute quantitative predictions of reactivity on a single crystal are required, the 6D-frozen-substrate approach is superior, and an exhaustive quantum mechanical study of a single surface is unavoidable. If, however, one is interested in understanding the trends between surfaces, the methods followed here should work at mid-to-high collision energies.

Considering only the direct pathway to dissociation on all eight crystals, two clear trends emerged. One favored corrugated surfaces over flat surfaces and the other favored 111-type steps over 100-type steps. The preference of 111-type steps over 100-type steps for reactivity has been corroborated with experimental data. We would encourage more accurate 6D classical simulations performed on a tractable system with a 111-type step such as Pt(331) (Pt(S)-[3(111) × (111)]) to confirm this trend. We developed a simple linear model that worked well in accounting for the reactivity differences over a wide range of different crystal facets. This leaves us with a framework for understanding some of the complex surfaces that one would likely encounter in industrial catalysis. A simple area-weighted-mean model works well, provided the reaction proceeds via a direct mechanism.

This approach begins to break down when precursor-mediated chemistry becomes important. For example, one facet of the surface may provide a molecularly trapped intermediate and another facet of the surface dissociates that intermediate. This is a direct form of coupling that would introduce a significant amount of nonlinearity into the system. However, under the high pressure and high concentration conditions used industrially, the surface is often littered with adatoms under typical operating

TABLE A1: Atom Parameters

	EEM parameters			bond-order correction				
atom type	χ (eV)	η (eV)	γ (Å)	$p_{ov/un}$	p_{val3}	p_{boc1}	p_{boc2}	p_{boc3}
H	3.845	10.084	0.891	−15.768	2.100	3.846	3.254	1.00
Pt	3.202	6.114	0.924	−6.966	1.847	5.00	2.579	0.00

TABLE A2: Bond Energy and Bond-Order Parameters

atom pair	D_e (kcal/mol)	p_{be1}	p_{be2}	r^{σ} (Å)	p_{bo1}	p_{bo2}
H−H	169.842	−0.359	9.312	0.687	−0.017	−5.941
H−Pt	169.457	−0.240	31.429	1.595	−0.088	9.646
Pt−Pt	109.633	−0.135	0.229	1.902	−0.107	5.220

TABLE A3: van der Waals Parameters

atom pair	R_{vdW} (Å)	ϵ (kcal/mol)	α	γ_{vdW}
H−H	1.353	0.062	9.386	5.001
Pt−H	1.755	0.029	11.805	5.481
Pt−Pt	2.028	0.280	12.516	6.008

TABLE A4: Angle Parameters

angle type	$\Theta_{o,o}$ (deg)[a]	k_a (kcal/mol)	k_b	$p_{v,2}$	λ_{12}
H−Pt−H	77.50	6.518	1.255	0.661	1.602
H−H−Pt	0.0	20.615	0.978	0.887	3.000
Pt−H−Pt	0.0	10.221	1.236	0.097	1.100
H−Pt−Pt	88.36	8.189	9.192	0.789	1.727
Pt−Pt−Pt	no angle interaction				

[a] The single-bond-order equilibrium angle is $180-\Theta_{o,o}$.

conditions. A follow up study by Gee et al.[29] showed that the indirect channel is significantly diminished in the presence of adsorbates. In light of this, the good performance of ReaxFF only in the direct region may not be that restrictive for engineering purposes. It may be possible that a few detailed studies of selected crystal facets and a simple linear model, like the one developed here, could accurately capture the dynamics of a complex catalyst because the role of indirect reaction channels may be diminished because of the preferential adsorption and the subsequent blocking of step sites.

Acknowledgment. We acknowledge partial support of this research by the U. S. Department of Energy, under award no. DE-FG02-03ER15468. However, any opinions, findings, conclusions, or recommendations expressed herein are those of the authors and do not necessarily reflect the views of the DOE.

Supporting Information Available: The convergence of sticking probability as a function of the number of trajectories and movies of sample reflected, dissociated, and trapped trajectories. This material is available free of charge via the Internet at http://pubs.acs.org.

References and Notes

(1) Ludwig, J.; Vlachos, D. G. *Mol. Simul.* **2004**, *30*, 765.
(2) Olsen, R. A.; Kroes, G. J.; Baerends, E. J. *J. Chem. Phys.* **1999**, *111*, 11155.
(3) Gee, A. T.; Hayden, B. E.; Mormiche, C.; Nunney, T. S. *J. Chem. Phys.* **2000**, *112*, 7660.
(4) Pasteur, A. T.; Dixon-Warren, S. J.; Ge, Q.; King, D. A. *J. Chem. Phys.* **1996**, *106*, 8896.
(5) Bonn, M.; Kleyn, A. W.; Kroes, G. J. *Surf. Sci.* **2002**, *500*, 475.
(6) Vincent, J. K.; Olsen, R. A.; Kroes, G. J.; Baerends, E. J. *Surf. Sci.* **2004**, *573*, 433.
(7) Persson, M.; Stromquist, J.; Bengtsson, L.; Jackson, B.; Shalashilin, D. V.; Hammer, B. *J. Chem. Phys.* **1999**, *110*, 2240.
(8) Busnengo, H. F.; Salin, A.; Dong, W. *J. Chem. Phys.* **2000**, *112*, 7641.
(9) Olsen, R. A.; Bãdescu, C.; Ying, S. C.; Baerends, E. J. *J. Chem. Phys.* **2004**, *120*, 11852.
(10) Olsen, R. A.; McCormack, D. A.; Baerends, E. J. *Surf. Sci.* **2004**, *571*, L325.
(11) McCormack, D. A.; Olsen, R. A.; Baerends, E. J. *J. Chem. Phys.* **2005**, *122*, 194708.
(12) van Duin, A. C. T.; Dasgupta, S.; Lorant, F.; Goddard, W. A. *J. Phys. Chem. A* **2001**, *105*, 9396.
(13) Feibelman, P. J. *Phys. Rev. B: Condens. Matter* **1995**, *52*, 16845.
(14) Tersoff, J. *Phys. Rev. B: Condens. Matter* **1988**, *37*, 6991.
(15) Brenner, D. W. *Phys. Rev. B: Condens. Matter* **1990**, *42*, 9458.
(16) Nielson, K. D.; van Duin, A. C. T.; Oxgaard, J.; Deng, W. Q.; Goddard, W. A. *J. Phys. Chem. A* **2005**, *109*, 493.
(17) Zhang, Q.; Cagin, T.; van Duin, A.; Goddard, W. A.; Qi, Y.; Hector, L. G. *Phys. Rev. B: Condens. Matter* **2004**, *69*.
(18) Cheung, S.; Deng, W. Q.; van Duin, A. C. T.; Goddard, W. A. *J. Phys. Chem. A* **2005**, *109*, 851.
(19) Chenoweth, K.; Cheung, S.; van Duin, A. C. T.; Goddard, W. A.; Kober, E. M. *J. Am. Chem. Soc.* **2005**, *127*, 7192.
(20) van Duin, A. C. T.; Strachan, A.; Stewman, S.; Zhang, Q. S.; Xu, X.; Goddard, W. A. *J. Phys. Chem. A* **2003**, *107*, 3803.
(21) Strachan, A.; Kober, E. M.; van Duin, A. C. T.; Oxgaard, J.; Goddard, W. A. *J. Chem. Phys.* **2005**, *122*.
(22) Strachan, A.; van Duin, A. C. T.; Chakraborty, D.; Dasgupta, S.; Goddard, W. A. *Phys. Rev. Lett.* **2003**, *91*.
(23) van Duin, A. C. T.; Zeiri, Y.; Dubnilova, F.; Kosloff, R.; Goddard, W. A., III. *J. Am. Chem. Soc.* **2005**, *127*, 11053.
(24) Han, S. S.; Kang, J. K.; Lee, H. M.; van Duin, A. C. T.; Goddard, W. A. *Appl. Phys. Lett.* **2005**, *86*.
(25) Chen, N.; Lusk, M. T.; van Duin, A. C. T.; Goddard, W. A. *Phys. Rev. B: Condens. Matter* **2005**, *72*.
(26) Han, S. S.; Kang, J. K.; Lee, H. M.; van Duin, A. C. T.; Goddard, W. A. *J. Chem. Phys.* **2005**, *123*.
(27) Han, S. S.; Kang, J. K.; Lee, H. M.; van Duin, A. C. T.; Goddard, W. A. *J. Chem. Phys.* **2005**, *123*.
(28) Han, S. S.; van Duin, A. C. T.; Goddard, W. A.; Lee, H. M. *J. Phys. Chem. A* **2005**, *109*, 4575.
(29) Gee, A. T.; Hayden, B. E.; Mormiche, C.; Nunney, T. S. *Surf. Sci.* **2002**, *512*, 165.
(30) Christmann, K.; Ertl, G.; Pignet, T. *Surf. Sci.* **1976**, *54*, 365.
(31) Salmeron, M.; Gale, R. J.; Somorjai, G. A. *J. Chem. Phys.* **1977**, *67*, 5324.
(32) Gale, R. J.; Salmeron, M.; Somorjai, G. A. *Phys. Rev. Lett.* **1977**, *38*, 1027.
(33) Christmann, K.; Ertl, G. *Surf. Sci.* **1976**, *60*, 365.
(34) Bernasek, S. L.; Siekhaus, W. J.; Somorjai, G. A. *Phys. Rev. Lett.* **1973**, *30*, 1202.
(35) Lin, T. H.; Somorjai, G. A. *J. Phys. Chem.* **1985**, *89*, 135.
(36) Lin, T. H.; Somorjai, G. A. *J. Chem. Phys.* **1984**, *81*, 704.
(37) Salmeron, M.; Gale, R. J.; Somorjai, G. A. *J. Chem. Phys.* **1979**, *70*, 2807.
(38) Somorjai, G. A. *Introduction to Surface Chemistry and Catalysis;* John Wiley & Sons: New York, 1994.
(39) Allen, M. P.; Tildesley, D. J. *Computer Simulation of Liquids;* Oxford University Press: New York, 1987.
(40) Berendsen, H. J. C.; Postma, J. P. M.; Vangunsteren, W. F.; Dinola, A.; Haak, J. R. *J. Chem. Phys.* **1984**, *81*, 3684.
(41) Kittel, C. *Introduction to Solid State Physics*, 7th ed.; Wiley: New York, 1995.
(42) Feibelman, P. J.; Hammer, B.; Nørskov, J. K.; Wagner, F.; Scheffler, M.; Stumpf, R.; Watwe, R.; Dumesic, J. A. *J. Phys. Chem. B* **2001**, *105*, 4018.
(43) Boettger, J. C. *Phys. Rev. B: Condens. Matter* **1994**, *49*, 16798.
(44) Scoles, G. *Atomic and Molecular Beam Methods;* Oxford University Press: New York, 1988; Vol. 1.
(45) Kolos, W.; Wolniewi. L. *J. Chem. Phys.* **1968**, *48*, 3672.
(46) Agresti, A.; Coull, B. A. *Am. Stat.* **1998**, *52*, 119.
(47) Luntz, A. C.; Brown, J. K.; Williams, M. D. *J. Chem. Phys.* **1990**, *93*, 5240.
(48) Samson, P.; Nesbitt, A.; Koel, B. E.; Hodgson, A. *J. Chem. Phys.* **1998**, *109*, 3255.